

Probing neutrino mass ordering with supernova neutrinos at $\text{NO}\nu\text{A}$ including the effect of sterile neutrinos

Papia Panda^{1,*} and Rukmani Mohanta^{1,†}

¹*School of Physics, University of Hyderabad, Hyderabad - 500046, India*

Abstract

In this work, we explore the possibility of probing the mass ordering sensitivity as a function of supernova distance in the context of the ongoing neutrino experiment $\text{NO}\nu\text{A}$. We provide a detailed study of the active-active and active-sterile mixing frameworks, illustrating how supernova neutrinos can be used to realize the existence of sterile neutrinos. Interestingly, we infer that observation of the NC channel alone can differentiate between the presence and absence of sterile neutrinos. Our results indicate that the primary channel of $\text{NO}\nu\text{A}$ can distinguish normal mass hierarchy from inverted mass hierarchy at 5σ confidence level for a supernova explosion occurring at a distance of 5 kpc. Additionally, we examine the impact of systematic uncertainties on mass hierarchy sensitivity, showing that higher levels of systematics lead to a reduction in sensitivity. Similarly, the inclusion of energy smearing significantly diminishes hierarchy sensitivity.

arXiv:2412.05213v2 [hep-ph] 13 Dec 2024

* ppapia93@gmail.com

† rmosp@uohyd.ac.in

I. INTRODUCTION

The core of a massive star with a mass greater than $8M_{\odot}$, where M_{\odot} is the mass of the sun, collapses with a tremendous amount of energy and light at the end of its life, producing a “core-collapse supernova”. Approximately 99% of this energy is carried away by neutrinos of various types, and their weakly interacting nature provides valuable insights into the supernova explosion mechanism.

The phenomenon of neutrino oscillation confirms that neutrinos possess non-zero masses. The flavour ($\nu_e, \nu_{\mu}, \nu_{\tau}$) and mass eigenstates (ν_1, ν_2, ν_3) of neutrinos are related by the unitary PMNS matrix, comprising of three mixing angles and one CP violating phase. Consequently, neutrino oscillation depends on six parameters: $\theta_{12}, \theta_{23}, \theta_{13}, \Delta m_{21}^2, \Delta m_{31}^2$, and δ_{CP} . Here, $\Delta m_{ij}^2 = m_i^2 - m_j^2$, and δ_{CP} is the CP-violating phase. These mixing parameters are determined very precisely except the CP phase δ_{CP} , the sign of Δm_{31}^2 , and the octant of atmospheric mixing angle θ_{23} . A positive Δm_{31}^2 indicates normal mass hierarchy (NH), while a negative sign implies inverted hierarchy (IH). In addition to long-baseline and reactor neutrino experiments, supernova neutrinos also present a highly effective option for addressing the mass hierarchy problem. This study aims to investigate the neutrino mass hierarchy problem using supernova neutrinos.

Some short-baseline neutrino experiments [1, 2] hint towards the existence of additional neutrino flavors, referred to as sterile neutrinos. However, experimental confirmation is not yet established. Sterile neutrinos, unlike active neutrinos, do not directly interact with Standard Model (SM) particles. Interactions among active neutrinos are described as the active-active framework, whereas interactions involving sterile neutrinos form the active-sterile framework. Information on the production, propagation, and detection of sterile neutrinos is limited, and one promising source for studying them is core-collapse supernovae. Several studies [3–20] have explored sterile neutrinos in supernovae, with some considering their presence at the core and others at the oscillation level. In this study, we assume that sterile neutrinos are produced during neutrino oscillations occurring in the region between the core and the surface of the supernova.

NO ν A (NuMI Off-axis ν_e Appearance) is a currently running long-baseline experiment which has the potential to detect supernova neutrinos during its operational period. Numerous studies [21–26] have simulated supernova neutrino events at NO ν A. The motivation for this work stems from the possibility of a supernova explosion occurring within the next few years. In such a scenario, the currently running long-baseline neutrino experiments, such as NO ν A or T2K, could extract valuable information from supernova neutrinos. While this study focuses on the NO ν A detector, a similar investigation could also be conducted using the T2K experiment. There are couple of work [27, 28] on the mass hierarchy in supernova neutrino in future neutrino experiments like DUNE, T2HK, T2HKK, and JUNO. These upcoming experiments with their larger detector volumes and higher statistics, are expected to provide deeper insights. However, they are likely to be in operation within a decade or more.

Here, we present an analysis of the prospects of observing supernova neutrinos at NO ν A in both the active-active and active-sterile frameworks, considering a single additional sterile neutrino.

The structure of the paper is outlined as follows. Sec. II provides a brief overview of the theory of supernova neutrino oscillations in both active-active and active-sterile frameworks. Sec. III details the experimental setup of the NO ν A detector and the simulation methodology employed in this study. In Sec. IV, the primary detection channels for supernova neutrinos are discussed. Sec. V presents the event rate calculations for various channels under both frameworks. The key findings of our study are summarized in Sec. VI, which is divided into three subsections: mass hierarchy sensitivity analysis, the impact of systematic uncertainties, and the influence of energy smearing on mass hierarchy sensitivity. Finally, Sec. VII concludes with our observations and final remarks.

II. THEORETICAL FORMALISM

During the initial phase of a supernova burst, electron-type neutrinos (ν_e) dominate, as they are primarily produced through electron capture on protons and nuclei when the neutrinosphere is affected by the shock wave [29]. These electron neutrinos interact strongly with matter, resulting in a lower average energy for ν_e compared to other neutrino types (ν_μ, ν_τ). Similarly, $\bar{\nu}_e$ neutrinos, which interact with matter via charged current interactions, also exhibit relatively low average energy, although it remains higher than that of ν_e . On the other hand, non-electron type neutrinos (ν_μ, ν_τ), commonly referred to as ν_x , are unable to interact via charged current at the energies of supernova neutrinos (a few MeV). These neutrinos interact only through neutral currents, resulting in the highest average energy for ν_x . In the primary neutrino spectra, the average energy hierarchy is expected to follow the relation [30]:

$$\langle E_{\nu_e}^0 \rangle < \langle E_{\bar{\nu}_e}^0 \rangle < \langle E_{\nu_x}^0 \rangle. \quad (1)$$

The flavor dependent primary neutrino spectra of the supernova neutrinos at the core can be expressed by power law distribution,

$$\Phi_\nu(E_\nu) = \mathcal{N} \left(\frac{E_\nu}{\langle E_\nu \rangle} \right)^\alpha e^{-(\alpha+1)\frac{E_\nu}{\langle E_\nu \rangle}}, \quad (2)$$

where E_ν and α are the neutrino energy and pinching parameter respectively. \mathcal{N} is the normalisation constant with the expression,

$$\mathcal{N} = \frac{(\alpha + 1)^{\alpha+1}}{\langle E_\nu \rangle \Gamma(\alpha + 1)}. \quad (3)$$

The flux at the core of the supernova can be written in terms of flavor dependent primary neutrino spectra $\Phi_\nu(E_\nu)$, average neutrino energy $\langle E_\nu \rangle$ and luminosity L_ν by the relation,

$$F_\nu^0 = \frac{L_\nu}{\langle E \rangle_\nu} \Phi_\nu(E_\nu). \quad (4)$$

In presence of Mikheyev-Smirnov-Wolfenstein (MSW) [31, 32] effect, the oscillated flux has the different expression in active-active and active-sterile framework. In the following subsections, we discuss the oscillated neutrino flux for these two neutrino frameworks respectively.

A. Active-active neutrino framework

The fluence at the detector on Earth in the active-active framework is expressed as:

$$\begin{aligned}
F_{\nu_e} &= pF_{\nu_e}^0 + (1 - p)F_{\nu_x}^0, \\
F_{\bar{\nu}_e} &= \bar{p}F_{\bar{\nu}_e}^0 + (1 - \bar{p})F_{\nu_x}^0, \\
2F_{\nu_x} &= (1 - p)F_{\nu_e}^0 + (1 + p)F_{\nu_x}^0, \\
2F_{\bar{\nu}_x} &= (1 - \bar{p})F_{\bar{\nu}_e}^0 + (1 + \bar{p})F_{\bar{\nu}_x}^0,
\end{aligned} \tag{5}$$

where p and \bar{p} represent the survival probabilities for electron neutrinos and electron antineutrinos, respectively and the corresponding expressions are provided in Table I. From the Table, we observe that p and \bar{p} have different values for normal and inverted mass orderings, which can thus yield a non-zero sensitivity to the mass hierarchy in this framework. One can further notice that the probabilities depend on the solar and reactor mixing angles, with no dependence on the atmospheric mixing angle θ_{23} . As a result, the fluence at the detector varies according to these two angles. Following Ref. [30], we have assumed the adiabatic condition for all our calculations, meaning that both the high-density and low-density flip probabilities, P_H and P_L , are zero inside the supernova.

Hierarchy	p	\bar{p}
Normal	$\sin^2 \theta_{13}$	$\cos^2 \theta_{12} \cos^2 \theta_{13}$
Inverted	$\sin^2 \theta_{12} \cos^2 \theta_{13}$	$\sin^2 \theta_{13}$

TABLE I: In active-active neutrino framework, survival probability expressions of neutrino (p) and antineutrino (\bar{p}) fluxes for two cases: normal hierarchy (NH) and inverted hierarchy (IH).

The fluence for different flavor neutrinos from Eqn.(5) are depicted graphically in Figure 1. To generate the panels of Figure 1, we use the values of the oscillation parameters as listed in Table III and have considered Garching electron capture supernova model [33] of our simulation. In this figure, the left (right) panel of upper row shows the time-integrated flux, or fluence, as a function of neutrino energy for $\nu_e(\bar{\nu}_e)$ across five different cases. Similarly, the left (right) panel of lower row illustrates the fluence of $\nu_x(\bar{\nu}_x)$ under varying conditions. In each panel, the red dashed-dotted curve represents the unoscillated data, while the purple (cyan) curve shows the fluence for normal (inverted) hierarchy in the active-active neutrino framework.

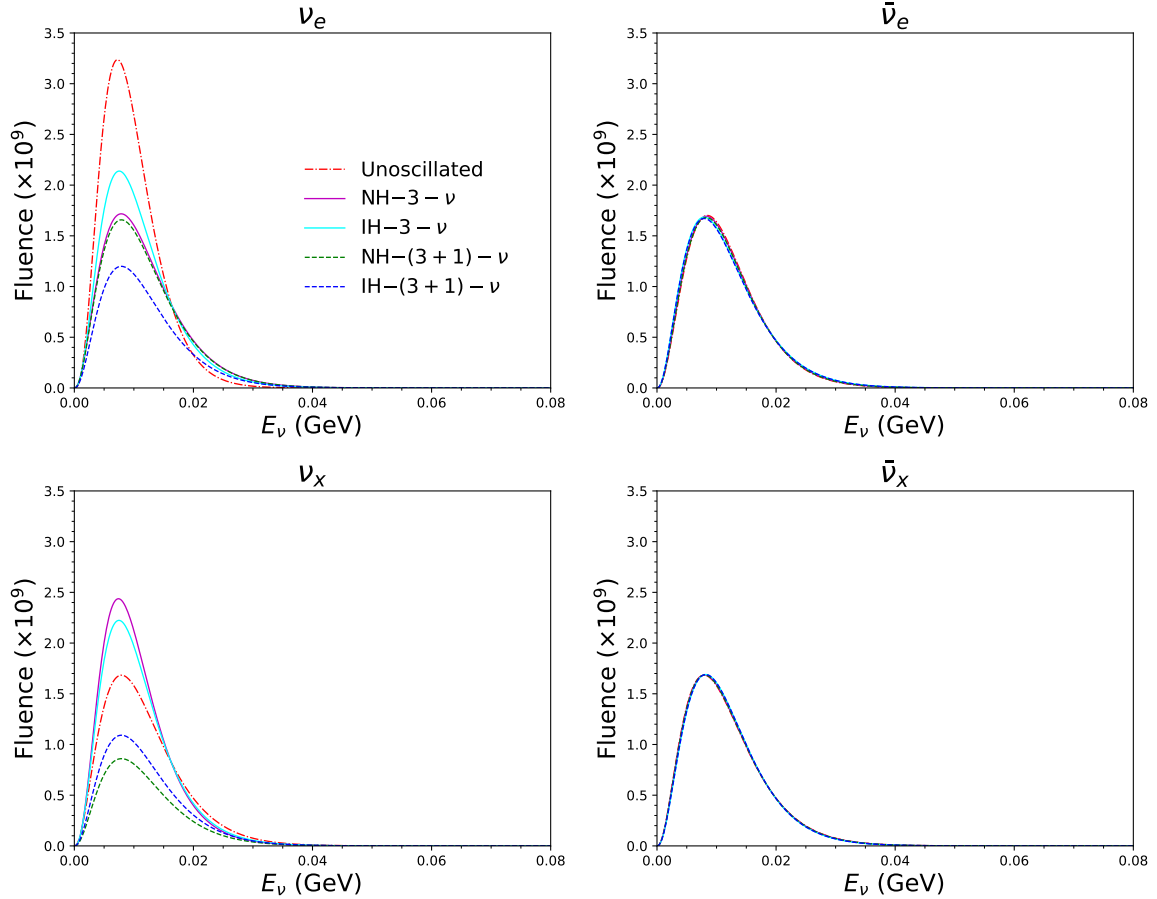


FIG. 1: Fluence (integrated flux over time) as a function of neutrino energy (E_ν) in GeV. Left (right) of upper row is for ν_e ($\bar{\nu}_e$) while left (right) of lower panel is for ν_x ($\bar{\nu}_x$) flavour. In each panel, color code is given in the legend.

From the left panel of the upper row, we observe that the red dash-dotted curve has a significantly higher fluence than the cyan and purple solid curves. Between the cyan and purple curves, the cyan curve is larger, indicating that for ν_e fluence, the inverted hierarchy (IH) results in higher fluence compared to the normal hierarchy (NH). Conversely, for the $\bar{\nu}_e$ case (right panel of the upper row), all cases appear to closely overlap, making it challenging to distinguish between them. In the leftmost panel of the bottom row, unlike the ν_e distribution, the red dash-dotted curve has a lower fluence compared to the cyan and purple solid curves. Compared to the cyan curve, the purple one is higher, showing that for ν_x fluence, the NH results in higher fluence than the IH. For the fluence of $\bar{\nu}_x$, similar to the that of $\bar{\nu}_e$, all the curves overlap, making it difficult to distinguish between them. The behavior observed in Figure 1 results from the interplay of two mixing angles, θ_{12} and θ_{13} , as well as the initial fluences of the different neutrino flavors.

B. Active-sterile neutrino framework

For active-sterile scenario, the expression for active and sterile neutrino fluxes are as follows [3]

$$\begin{aligned}
F_{\nu_e} &= a_{ee}F_{\nu_e}^0 + a_{ex}F_{\nu_x}^0 + a_{es}F_{\nu_s}^0, \\
F_{\bar{\nu}_e} &= b_{ee}F_{\bar{\nu}_e}^0 + b_{ex}F_{\bar{\nu}_x}^0 + b_{es}F_{\bar{\nu}_s}^0, \\
2F_{\nu_x} &= (a_{\mu e} + a_{\tau e})F_{\nu_e}^0 + (a_{\mu x} + a_{\tau x})F_{\nu_x}^0 + (a_{\mu s} + a_{\tau s})F_{\nu_s}^0, \\
2F_{\bar{\nu}_x} &= (b_{\mu e} + b_{\tau e})F_{\bar{\nu}_e}^0 + (b_{\mu x} + b_{\tau x})F_{\bar{\nu}_x}^0 + (b_{\mu s} + b_{\tau s})F_{\bar{\nu}_s}^0, \\
F_{\nu_s} &= a_{se}F_{\nu_e}^0 + a_{sx}F_{\nu_x}^0 + a_{ss}F_{\nu_s}^0, \\
F_{\bar{\nu}_s} &= b_{se}F_{\bar{\nu}_e}^0 + b_{sx}F_{\bar{\nu}_x}^0 + b_{ss}F_{\bar{\nu}_s}^0,
\end{aligned} \tag{6}$$

where the expressions of $a_{\alpha e}$, $a_{\alpha x}$, $b_{\alpha e}$ and $b_{\alpha x}$ are given in Eq. 7. We further assume there are no initial sterile neutrinos at the core of the supernova, so $F_{\nu_s}^0$ and $F_{\bar{\nu}_s}^0$ are zero and

$$\begin{aligned}
a_{\alpha e} &= |U_{\alpha 1}|^2 P_H P_L (1 - P_S) + |U_{\alpha 3}|^2 P_S + |U_{\alpha 2}|^2 P_H (1 - P_L) (1 - P_S) \\
&\quad + |U_{\alpha 4}|^2 (1 - P_S) (1 - P_H) \\
a_{\alpha x} &= |U_{\alpha 1}|^2 (1 - P_H P_L) + |U_{\alpha 2}|^2 (1 - P_H + P_H P_L) + |U_{\alpha 4}|^2 P_H \\
b_{\alpha e} &= |U_{\alpha 1}|^2 \\
b_{\alpha x} &= |U_{\alpha 2}|^2 + |U_{\alpha 3}|^2
\end{aligned} \tag{7}$$

for normal hierarchy. For the inverted hierarchy case, the expressions are,

$$\begin{aligned}
a_{\alpha e} &= |U_{\alpha 1}|^2 P_L (1 - P_S) + |U_{\alpha 2}|^2 P_S + |U_{\alpha 4}|^2 (1 - P_S) (1 - P_L) \\
a_{\alpha x} &= |U_{\alpha 1}|^2 (1 - P_L) + |U_{\alpha 3}|^2 + |U_{\alpha 4}|^2 P_L \\
b_{\alpha e} &= |U_{\alpha 2}|^2 \bar{P}_H + |U_{\alpha 3}|^2 (1 - \bar{P}_H) \\
b_{\alpha x} &= |U_{\alpha 1}|^2 + |U_{\alpha 2}|^2 (1 - \bar{P}_H) + |U_{\alpha 3}|^2 \bar{P}_H.
\end{aligned} \tag{8}$$

Similar to active-active condition, here also, in adiabatic approximation, survival probabilities of electron (anti)neutrino in high and low densities are set to be zero, i.e., $P_H = \bar{P}_H = P_L = \bar{P}_L = P_S = \bar{P}_S = 0$. The 4×4 mixing matrix can be parametrized as $U_{\alpha i} = R_{14} \cdot R_{23} \cdot R_{13} \cdot R_{12}$ ordering, where R_{ij} are the rotation matrices in $i - j$ plane, can be expressed as [3],

$$U_{\alpha i} = \begin{pmatrix} c_{12}c_{13}c_{14} & s_{12}c_{13}c_{14} & s_{13}c_{14} & s_{14} \\ -s_{12}c_{23} - c_{12}s_{23}s_{13} & c_{12}c_{23} - s_{12}s_{23}s_{13} & s_{23}c_{13} & 0 \\ s_{12}s_{23} - c_{12}c_{23}s_{13} & -c_{12}s_{23} - s_{12}c_{23}s_{13} & c_{23}c_{13} & 0 \\ -c_{12}c_{13}s_{14} & -s_{12}c_{13}s_{14} & -s_{13}s_{14} & c_{14} \end{pmatrix}, \tag{9}$$

where, $c(s)_{23} = \cos \theta_{23} (\sin \theta_{23})$ and so on. Under the adiabatic condition, the expressions of $a_{\alpha e(x)}$ and $b_{\alpha e(x)}$ are given in Table II. Depending upon the values of the mixing angles and

Hierarchy	$a_{\alpha e}$	$a_{\alpha x}$	$b_{\alpha e}$	$b_{\alpha x}$
Normal	$ U_{\alpha 4} ^2$	$ U_{\alpha 1} ^2 + U_{\alpha 2} ^2$	$ U_{\alpha 1} ^2$	$ U_{\alpha 2} ^2 + U_{\alpha 3} ^2$
Inverted	$ U_{\alpha 4} ^2$	$ U_{\alpha 1} ^2 + U_{\alpha 3} ^2$	$ U_{\alpha 3} ^2$	$ U_{\alpha 1} ^2 + U_{\alpha 2} ^2$

TABLE II: In the active-sterile neutrino framework, the expressions for the couplings of neutrinos ($a_{\alpha e}, a_{\alpha x}$) and anti-neutrino ($b_{\alpha e}, b_{\alpha x}$) are provided for two scenarios: normal hierarchy (NH) and inverted hierarchy (IH).

the initial fluence of different flavours, the eq. 6 has different values in normal and inverted scenario. It is noteworthy that, the coupling of (anti)neutrinos depends on all the mixing angles: $\theta_{12}, \theta_{13}, \theta_{23}$, and θ_{14} , as seen from Table II. Thus, the presence of a sterile neutrino offers the possibility of gaining insight into the octant sensitivity of θ_{23} through supernova neutrinos. This is in contrast to the active-active framework, where θ_{23} does not appear in the expressions of p and \bar{p} .

The expressions in eq. 6 are graphically represented in Fig. 1. To generate the panels in Fig. 1, we use the sterile neutrino oscillation parameters listed in Table III. In this figure, the green and blue dashed curves represent the fluence for active-sterile neutrino scenario. The green dashed curve corresponds to the NH, while the blue dashed curve represents the IH.

In the left panel of the upper row, we observe that the red dash-dotted curve is significantly higher than the green and blue dashed curves. Comparing the green and blue curves, we find that, unlike the active-active framework, for active-sterile scenario, the NH spectrum is higher than the IH spectrum. For the $\bar{\nu}_e$ case, all the expressions appear to overlap closely, making them indistinguishable. In the left panel of the bottom row, similar to the ν_e distribution, the red dash-dotted curve shows a higher fluence compared to the green and blue dashed curves. When comparing the green and blue curves, the blue curve is higher than the green. For $\bar{\nu}_x$, the blue, green dashed, and red dash-dotted curves overlap, making it difficult to distinguish between the NH and IH results.

It is worth comparing the active-active scenario with the active-sterile framework. Based on Fig. 1, we can draw the following conclusions:

- For the ν_e flux, the active-active scenario is always greater than the active-sterile framework across the entire energy range, regardless of whether the ordering is normal or inverted.
- The behavior for the $\bar{\nu}_e$ flux is exactly the same as that for the ν_e flux.
- Similarly, the ν_x flux exhibits the same behavior as the ν_e flux.
- For the $\bar{\nu}_x$ flux, the active-active scenario flux and the active-sterile framework flux completely overlap across the entire energy range.

From the observations above, a distinct feature emerges for $\bar{\nu}_x$, where, unlike other fluence characteristics, the fluence in the active-sterile scenario overlaps with that of the active-active framework. This behavior is evident in neutral current (NC) channels, which we discuss in the following sections.

In our calculations, we have considered only the Mikheyev-Smirnov-Wolfenstein (MSW) effect [30]. However, within the supernova, numerous flavor-changing processes occur. One significant effect following the MSW effect is the “collective effect”. Extensive studies [29, 34–36] have explored the collective effect in supernova neutrinos, but its outcomes remain largely uncertain. We currently have limited knowledge about the collective effect, including the type of its nature, mechanisms, and behavior. Due to this lack of a clear understanding, we have not included the collective effect in our calculations of fluence for different neutrino flavors.

III. EXPERIMENTAL SETUP AND SIMULATION DETAILS

In this section, we discuss the key features of the NO ν A detector and the simulation tools utilized in our study. The NuMI Off-axis ν_e Appearance (NO ν A) experiment [37–42] is a long-baseline accelerator neutrino experiment currently in operation. It employs two functionally identical detectors: one near detector and one far detector. Both detectors are constructed using planes of extruded polyvinyl chloride (PVC) with a custom formulation that includes titanium dioxide, with ^{12}C as the primary component [43]. The fiducial volumes of the near and far detectors are 300 tons and 14 kilotons, respectively. The far detector, being nearly 50 times larger than the near detector, is significantly more sensitive to signals from supernova neutrinos. As a result, we focus on the far detector for the remainder of our simulations. For our simulations, we use the Supernova Neutrino Observatories with GLoBES (SNOWGLoBES) software [45], which is based on the GLoBES framework [46, 47]. This tool is specifically designed to study supernova neutrinos. SNOWGLoBES calculates

Oscillation parameters	Values
θ_{12}	33.41°
θ_{13}	8.58°
θ_{23}	42.20°
θ_{14}	5°
Δm_{21}^2	$7.410 \times 10^{-5} \text{ eV}^2$
Δm_{31}^2	$\pm 2.507 \times 10^{-3} \text{ eV}^2$
Δm_{41}^2	1 eV^2

TABLE III: Neutrino oscillation parameter values [44] used in the study.

event rates by utilizing input parameters such as neutrino fluxes, cross sections, and detector configurations. For calculating mass hierarchy sensitivity, we apply the Poisson log-likelihood statistical formula, given by the expression:

$$\chi_{\text{stat}}^2 = 2 \sum_{i=1}^n \left[N_i^{\text{test}} - N_i^{\text{true}} - N_i^{\text{true}} \log \left(\frac{N_i^{\text{test}}}{N_i^{\text{true}}} \right) \right], \quad (10)$$

where N_i^{true} and N_i^{test} are the event rates of true and test spectrum respectively. To evaluate the impact of systematic errors on physics sensitivities, we consider two types of errors: normalization error and energy calibration error. The normalization error affects the overall amplitude of the spectrum while preserving its structure. In contrast, the energy calibration error varies with the energy value of each bin, altering the shape of the event spectrum. When both errors are included, the test event rate is expressed as:

$$N_i^{\text{test}} \rightarrow N_i^{\text{test}} [(1 + a) + b(E'_i - \bar{E}') / (E'_{\text{max}} - E'_{\text{min}})], \quad (11)$$

Here, a and b are the nuisance parameters corresponding to the normalization and energy calibration errors, respectively. For a 5% systematic error in both types, the nuisance parameters a and b can be expressed in terms of the pull variables p_1 and p_2 as

$$a = 0.05 p_1, \quad b = 0.05 p_2. \quad (12)$$

Finally, in presence of systematics errors [48], the final expression of sensitivity is,

$$\chi_{\text{stat+sys}}^2 = \chi_{\text{stat}}^2 + p_1^2 + p_2^2. \quad (13)$$

IV. MAIN CHANNELS

Since the far detector of NO ν A is a scintillator detector, the primary interaction with supernova neutrinos is through inverse beta decay (IBD). In this process, an electron antineutrino interacts with a proton, resulting in the production of a neutron and a positron, as represented by the following equation,

$$\bar{\nu}_e + p = n + e^+. \quad (14)$$

We refer to this interaction channel as ‘‘Channel (i)’’. Another prominent channel involves the interaction of an electron antineutrino with ^{12}C , resulting in the production of a positron and ^{12}B ,

$$\bar{\nu}_e + {}^{12}\text{C} = e^+ + {}^{12}\text{B}. \quad (15)$$

This interaction is named as ‘‘Channel (ii)’’. The third significant channel involves the interaction of an electron neutrino with ^{12}C , resulting in the production of ^{12}N and an electron

$$\nu_e + {}^{12}\text{C} = e^- + {}^{12}\text{N}. \quad (16)$$

Channel	Framework: $3\nu/(3+1)\nu$	Hierarchy	Event Number
Channel (i) (IBD)	3ν	NH	129665
		IH	133128
	$(3+1)\nu$	NH	128679
		IH	132117
Channel (ii) ($\bar{\nu}_e - C^{12}$)	3ν	NH	3856.54
		IH	4411.67
	$(3+1)\nu$	NH	3827.24
		IH	4378.15
Channel (iii) ($\nu_e - C^{12}$)	3ν	NH	3809.95
		IH	2996.25
	$(3+1)\nu$	NH	3767.84
		IH	2713.18
Channel (iv) ($\nu_e - e$)	3ν	NH	1123.14
		IH	1178.39
	$(3+1)\nu$	NH	1095.48
		IH	791.09

TABLE IV: Event numbers for different channels (Channel (i), Channel (ii), Channel (iii), and Channel (iv)) at a supernova distance of 1 kpc. NH (normal hierarchy) and IH (inverted hierarchy) represent the mass hierarchy, while 3ν [$(3+1)\nu$] represents the active-active [active-sterile] neutrino framework.

This channel we term as ‘‘Channel (iii)’’. Lastly, there is the elastic scattering interaction between an electron neutrino and an electron in the detector:

$$\nu_e + e^- = \nu_e + e^- . \quad (17)$$

This channel is referred as ‘‘Channel (iv)’’.

In addition to these four channels, we also consider neutral current (NC) interactions between various flavor neutrinos and ^{12}C . The importance of including neutral current interactions lies in the fact that, in the presence of a sterile neutrino, the NC event rates differ, as some $\nu_e(\bar{\nu}_e)$ can convert to $\nu_s(\bar{\nu}_s)$ with a non-zero probability. This conversion results a difference in event numbers between the active-active neutrino case and the active-sterile neutrino scenario. All possible neutral current interactions are listed in Table V, which provides the event numbers for each type of NC channel at a distance of 1 kpc, for both normal and inverted mass orderings. The Table includes scenarios for both the active-active neutrino case and the active-sterile neutrino framework. The differences in event

Framework: $3\nu/(3+1)\nu$	Hierarchy	$\nu_e -^{12} C$	$\bar{\nu}_e -^{12} C$	$\nu_\mu -^{12} C$	$\bar{\nu}_\mu -^{12} C$	$\nu_\tau -^{12} C$	$\bar{\nu}_\tau -^{12} C$	Total NC
3ν	NH	2274.80	2019.66	1533.19	2242.18	1533.19	2242.18	11845.21
	IH	1838.70	2300.71	1751.24	2101.66	1751.24	2101.66	11845.21
$(3+1)\nu$	NH	2247.06	2004.31	1180.84	2242.18	1180.84	2242.18	11097.41
	IH	1618.02	2283.22	1497.76	2101.66	1497.76	2101.66	11100.08

TABLE V: The event rates for six types of neutral current channels at a supernova distance of 1 kpc for different mass hierarchy cases: NH and IH. 3ν [$(3+1)\nu$] represents the active-active [active-sterile] neutrino framework.

rates between these scenarios highlight the need to explore the impact of sterile neutrinos on supernova neutrino oscillations.

V. EVENT RATES

In this section, we present the event rate distribution as a function of neutrino energy for the active-active scenario, and the active-sterile framework. Tables IV and V display the event rates for both normal and inverted hierarchies in both the scenarios.

In the first subsection, we present the event rate distribution as a function of neutrino energy for Channels (i), (ii), (iii), and (iv) in the active-active scenario. The second subsection covers the event rate distribution for the channels mentioned above in the active-sterile scenario. In the next subsection, we also provide a detailed discussion of the neutral current channel to offer a comprehensive view.

A. Active-active Neutrino Framework

Table IV shows the event numbers for the four different channels, assuming the supernova is located at a distance of 1 kpc. The first two rows for each channel represent the total event numbers for the active-active scenario, with both NH and IH conditions. From the Table, we observe that the total event number for Channel (i) is significantly higher than for Channel (ii), while the event numbers for Channel (iii) are relatively close to those of Channel (ii). In comparison, Channel (iv) has a much lower event count than Channel (iii) for both NH and IH conditions.

Similarly, the red and green curves in each panel of Fig. 2 visually illustrate the variation in event rates as a function of neutrino energy. From both Table IV and Fig. 2, we observe that for Channel (i), there is a very small difference between the event rates for NH and IH. In Channel (ii), a significant difference emerges in the event rate spectrum after 10 MeV neutrino energy, with the IH event rates being higher than the NH rates. For Channel (iii),

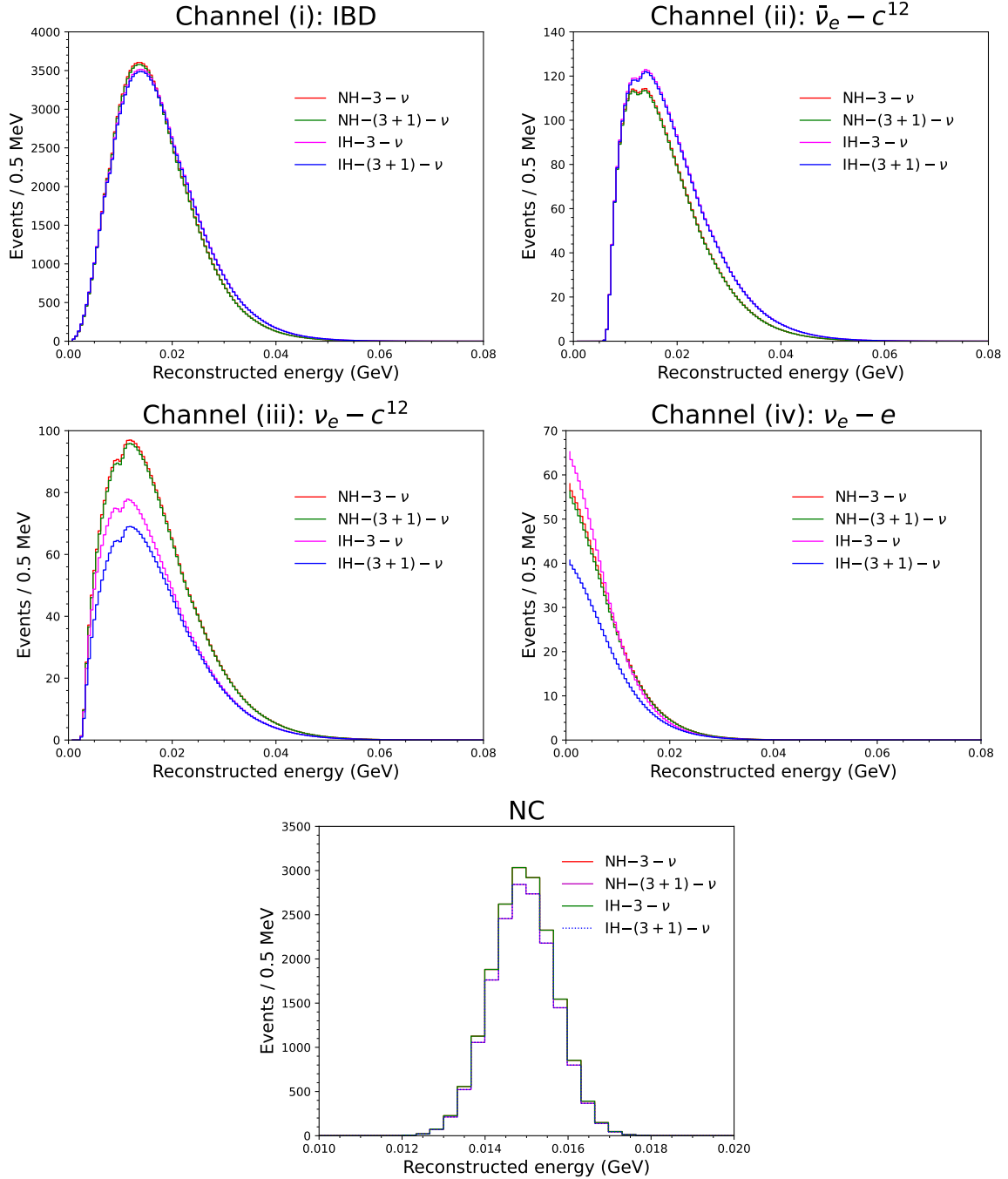


FIG. 2: Event rate in active-active and active-sterile frameworks for five different channels for supernova at a distance of 1 kpc. Color codes are given in the legend. NH (IH) represents the normal (inverted) hierarchy.

the event rates are higher for NH compared to IH. In contrast, for Channel (iv), the IH event rates are higher than the NH event rates.

To understand the characteristics of the event rate spectrum, we focus on the fluence spectrum shown in Fig. 1. For the event rate spectrum of Channel (i), we examine the

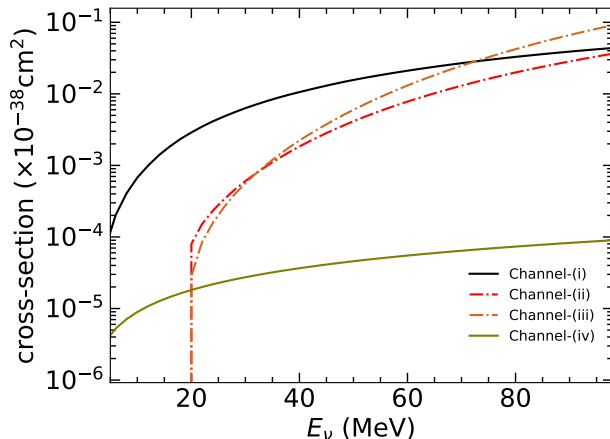


FIG. 3: Cross section for different channels of No ν A detector.

fluence of $\bar{\nu}_e$ in Fig. 1. It is observed that for $\bar{\nu}_e$, the fluences for NH and IH overlap, which explains the event rate spectrum behavior for Channel (i). Similarly, for Channel (ii), we again focus on the $\bar{\nu}_e$ fluence. In this case, we see that the event rate for the inverted hierarchy is higher than that for the normal hierarchy. This is due to the interplay between the fluence and the cross-section of Channel (ii). The event rate is proportional to the product of the fluence and the cross-section for the particular channel.

To better understand the behavior of the cross-sections for different channels with respect to neutrino energy, we have plotted Figure 3, where the black, red dot-dashed, brown dot-dashed, and green curves represent the cross-sections for Channels (i), (ii), (iii), and (iv), respectively. In this figure, the IBD cross-section is the largest, followed by Channels (iii), (ii), and (iv). The multiplication of the cross-section and the corresponding fluence results in the event rate spectrum for each channel. Turning to Channel (iii), this channel involves the interaction of an electron neutrino with ^{12}C . In this case, we focus on the ν_e fluence, and here the IH fluence is higher than the NH fluence. However, when the cross-section is multiplied by the fluence, the event rate for NH becomes greater than that for IH.

Finally, Channel (iv) corresponds to the elastic scattering of an electron with an electron neutrino. It is interesting to note that the event rate behavior for Channel (iv) differs from the other channels. This difference is attributed to the smearing effect in the detector. If the smearing effects were removed, the event rate behavior would resemble that of the other channels.

B. Active-sterile neutrino framework

In this subsection, we present the event rates in the active-sterile framework. The last two rows of each channel in Table IV show the event numbers for the active-sterile scenario. It is evident that in the presence of a sterile neutrino, the detected event rate decreases, as some

of the active neutrinos oscillate into the undetected sterile neutrinos. Table IV indicates that, for both NH and IH conditions, the event number in the active-sterile scenario is lower than that in the active-active scenario.

The results from Table IV are graphically represented in Fig. 2. In each panel of Fig. 2, the green and blue solid curves represent the event rates for the NH and IH active-sterile neutrino frameworks, respectively. The explanations for the curves in each channel are similar to those provided for the active-active framework.

C. NC channels

Now, we discuss the neutral current event rates for both the active-active and active-sterile scenarios. Neutral current interactions apply to all neutrino flavors. In our calculation, we have considered the interactions of all neutrino flavors with ^{12}C , as the primary material in the NO ν A detector is Carbon-12. Table V presents the event numbers for each neutral current interaction channel at a supernova distance of 1 kpc. The first [last] two rows of the Table show the event rates for the interaction channels in the active-active [active-sterile] scenario. In the last column of Table V, we provide the total event rates for all six channels and display the change in the total event rate between the normal and inverted hierarchy conditions.

From the Table, we observe that, for all channels except the NC events involving $\bar{\nu}_x$, the event rate in the active-sterile scenario is lower than in the active-active framework. This is expected, as the presence of a sterile neutrino allows some of the active neutrinos to oscillate into sterile neutrinos, resulting in fewer NC events compared to the scenario where sterile neutrinos are not considered. However, it is interesting to note that the NC event rate for the $\bar{\nu}_x - ^{12}\text{C}$ channel is same in the active-sterile scenario as in the active-active case, which holds true for both normal and inverted mass ordering. Now let us examine this nature further. The event rate is proportional to the product of the fluence and the cross-section. First, in the left panel of upper row of Fig. 4, we plot the cross-section for the $\bar{\nu}_x - ^{12}\text{C}$ channel, which increases with energy. We then examine the plot of the fluence of $\bar{\nu}_x$ for both frameworks in right panel of upper row of Fig. 4. The panel shows exactly overlapping of the two fluences over full energy range. This behavior is consistent for both normal and inverted orderings. As a result, when the fluence is multiplied by the cross-section, the event rate becomes exactly same for the active-sterile scenario with active-active framework.

To understand why the $\bar{\nu}_x$ fluence is same in the active-active scenario as the active-sterile case, we examine the expression for the fluence of $F_{\bar{\nu}_x}$, which depends on $F_{\bar{\nu}_e}^0$ and $F_{\bar{\nu}_x}^0$. In the active-active scenario with normal ordering, the fluence is given by (from eq. 5)

$$F_{\bar{\nu}_x} = 0.9777F_{\bar{\nu}_e}^0 + 1.0222F_{\bar{\nu}_x}^0 . \quad (18)$$

In the active-sterile scenario with normal ordering, the expression becomes (from eq. 6 and

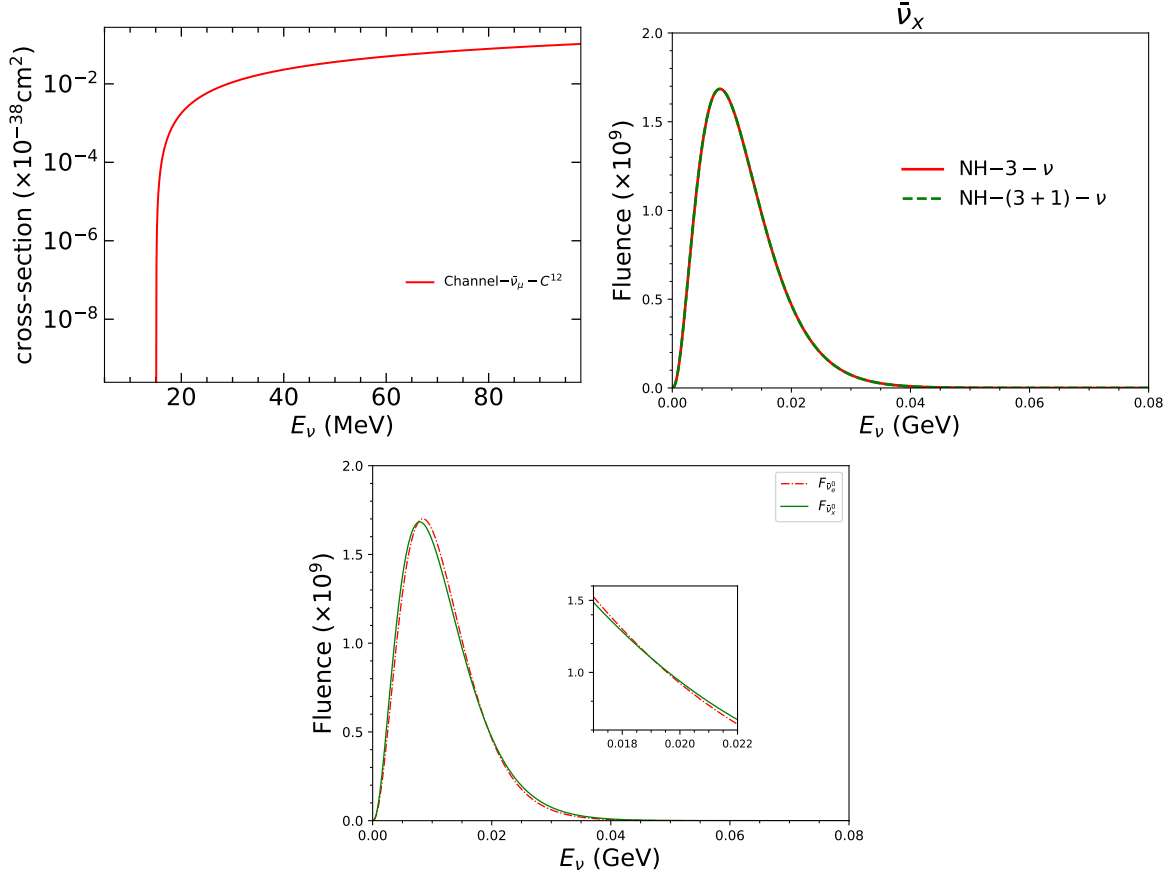


FIG. 4: Left panel of upper row: cross section of the NC channel $\bar{\nu}_\mu - {}^{12}\text{C}$, right panel of upper row: fluence of $\bar{\nu}_x$ for active-active and active-sterile framework considering normal hierarchy, lower row: fluence of $\bar{\nu}_e^0$ and $\bar{\nu}_x^0$ as a function of neutrino energy.

assuming initially no sterile neutrino is present at the core)

$$F_{\bar{\nu}_x} = 0.3184F_{\bar{\nu}_e}^0 + 1.6813F_{\bar{\nu}_x}^0 . \quad (19)$$

Both the above equation is calculated with the help of oscillation parameter values given in Table III.

The lower panel of Fig. 4 shows the unoscillated fluences of $\bar{\nu}_e^0$ and $\bar{\nu}_x^0$ as a function of energy. It demonstrates that from 0 to 0.01 GeV energy range, $F_{\bar{\nu}_x}^0$ is greater than $F_{\bar{\nu}_e}^0$, however after that and upto 0.016 GeV energy $F_{\bar{\nu}_x}^0$ gets smaller than $F_{\bar{\nu}_e}^0$. Beyond 0.016 GeV, $F_{\bar{\nu}_e}^0$ becomes smaller than $F_{\bar{\nu}_x}^0$. Thus, we can conclude that the interplay between the initial fluences, $F_{\bar{\nu}_e}^0$ and $F_{\bar{\nu}_x}^0$, along with the survival probability values, leads to the same event rate in the active-sterile framework as in the active-active scenario for the $\bar{\nu}_x - {}^{12}\text{C}$ channel.

VI. RESULTS

In this section we show the main results of our work for both the neutrino frameworks. We divide our results into some important subsections while in each subsection, we illustrate the results drawn from active-active scenario first, and then talk about the results from the active-sterile framework.

A. Mass hierarchy sensitivity

The sensitivity to the neutrino mass hierarchy refers to an experiment's ability to distinguish between normal and inverted mass hierarchy in the neutrino spectrum. Supernovae, being prolific sources of neutrinos, provide an excellent opportunity to probe the mass hierarchy. This can be achieved through currently operating long-baseline neutrino experiments, such as $\text{NO}\nu\text{A}$. In this subsection, we discuss how the mass hierarchy sensitivity varies as a function of the supernova distance (measured in kiloparsecs).

The key findings are presented in Fig. 5. Each panel illustrates the mass hierarchy sensitivity as a function of the supernova distance for various detection channels. In our analysis, we consider four primary channels along with the NC channel, and the results for all five channels are shown in Fig. 5 under four different scenarios. For the case labeled $3 - \nu - \text{true-NH}$ (IH), the analysis assumes a active-active scenario with the true spectrum having normal (inverted) hierarchy and the test spectrum as inverted (normal) hierarchy. Similarly, the condition $(3 + 1) - \nu - \text{true-NH}$ (IH) corresponds to the active-sterile framework, where the true spectrum has a normal (inverted) hierarchy and the test spectrum with inverted (normal) hierarchy.

In each panel, the red dashed (green dot-dashed) curve represents the mass hierarchy sensitivity for the active-active (active-sterile) scenario with normal hierarchy in the true spectrum. Likewise, the cyan solid (blue dashed) curve shows the results for the active-active (active-sterile) scenario with inverted hierarchy in the true spectrum. The brown dotted line indicates the 5σ confidence level threshold for mass hierarchy sensitivity. From Fig. 5, we observe that sensitivity is generally higher when the true spectrum assumes as inverted hierarchy compared to normal hierarchy. Examining the individual channels we found that for channels (i) and (ii), both active-active and active-sterile scenarios produce nearly identical results. However, for channels (iii) and (iv), a clear distinction emerges, with the active-sterile framework showing a higher sensitivity than the active-active scenario. This behavior can be explained using Table IV, which highlights a significant discrepancy in event numbers between normal and inverted hierarchies for the active-sterile framework. In contrast, the active-active scenario exhibits minimal differences in event numbers between these hierarchies.

For the NC channel, as the event rate for NH and IH condition of active-active scenario

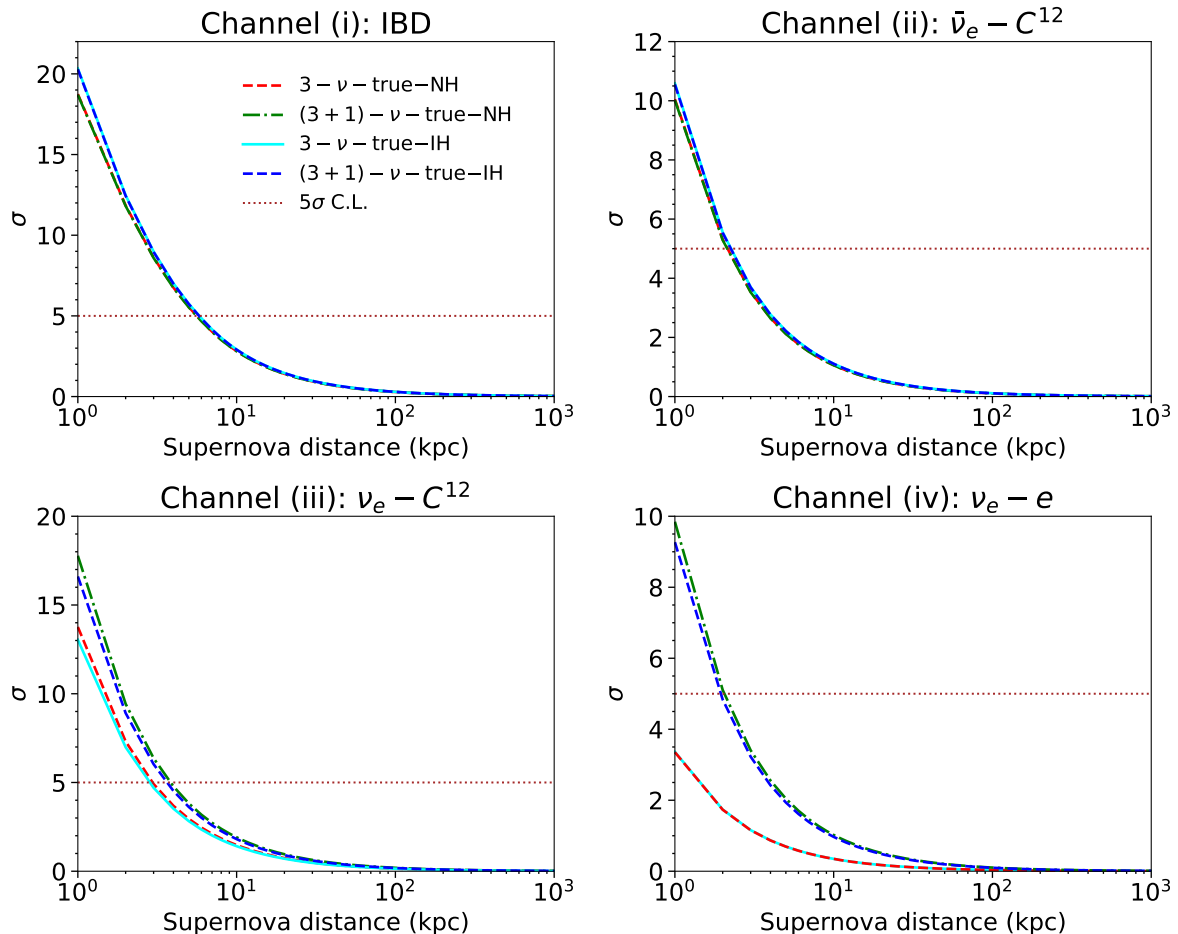


FIG. 5: Mass ordering sensitivity as a function of supernova distance (in kpc). Color code are given in the legends.

is same in number, there is no mass hierarchy sensitivity from this channel. However, in the active-sterile framework, a non-zero difference between NH and IH event rates introduces some mass hierarchy sensitivity. Since the difference in event numbers for NH and IH in the active-sterile framework is small for the $\text{NO}\nu\text{A}$ detector, this setup does not offer significant mass hierarchy sensitivity. Notably, future long-baseline experiments with much larger far detector volumes are expected to show a significant difference in event numbers between the active-active and active-sterile scenarios, as well as between NH and IH event rates in the active-sterile framework, leading to significant mass hierarchy sensitivity from the NC channel. Thus, the NC channel emerges as a valuable tool for investigating the possible existence of sterile neutrinos in nature.

In conclusion, the results indicate that using only the IBD channel, $\text{NO}\nu\text{A}$ can discriminate the correct mass ordering from the incorrect one at the 5σ confidence level for a supernova located approximately 5 kpc away. Also, we can effectively study sterile neutrinos, particularly using neutrinos from supernovae.

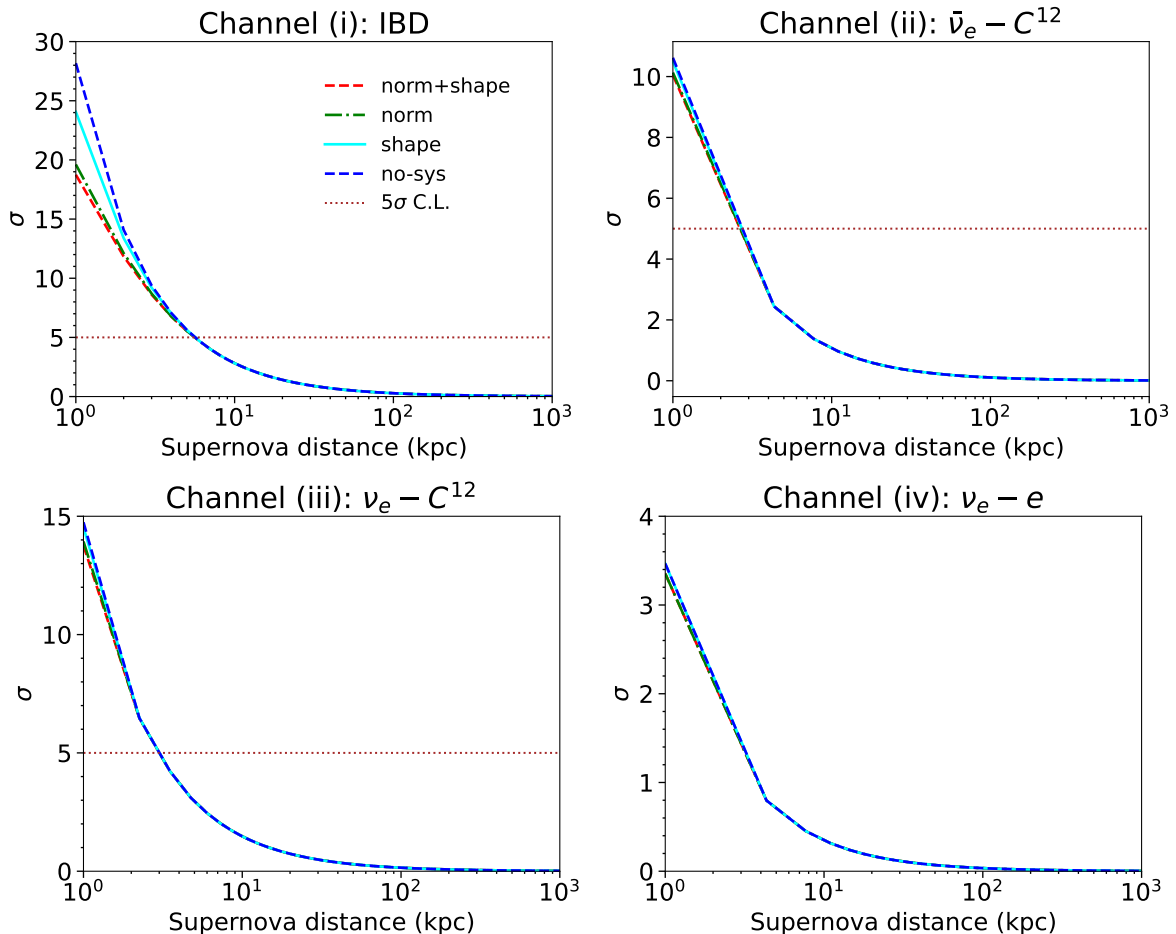


FIG. 6: Mass hierarchy sensitivity as a function of supernova distance (in kpc) for all four channels in different systematics uncertainty conditions; “norm” (“shape”) stands for normalization (energy calibration) error. This figure is for active-active framework, however similar nature is for active-sterile scenario. Color codes are given in the legend.

B. Effect of systematics

In this subsection, we examine the impact of systematic uncertainties on mass hierarchy sensitivity as a function of supernova distance. These uncertainties arise from various sources, including supernova flux measurements, cross-section measurements, and the incoming neutrino direction. To analyze these effects, we present Fig. 6, where each channel is shown with curves corresponding to different combinations of systematic errors. The Figure shows the results for active-active scenario only. Similar effect can be seen in active-sterile framework as well.

In our analysis, we consider two types of errors: normalization and energy calibration. In each panel, “norm” represents normalization uncertainties, while “shape” corresponds to energy calibration uncertainties. For the cyan (green dot-dashed) curve, we set p_1 (p_2) to zero in Eq. 13. The red dashed curve includes contributions from both p_1 and p_2 in the

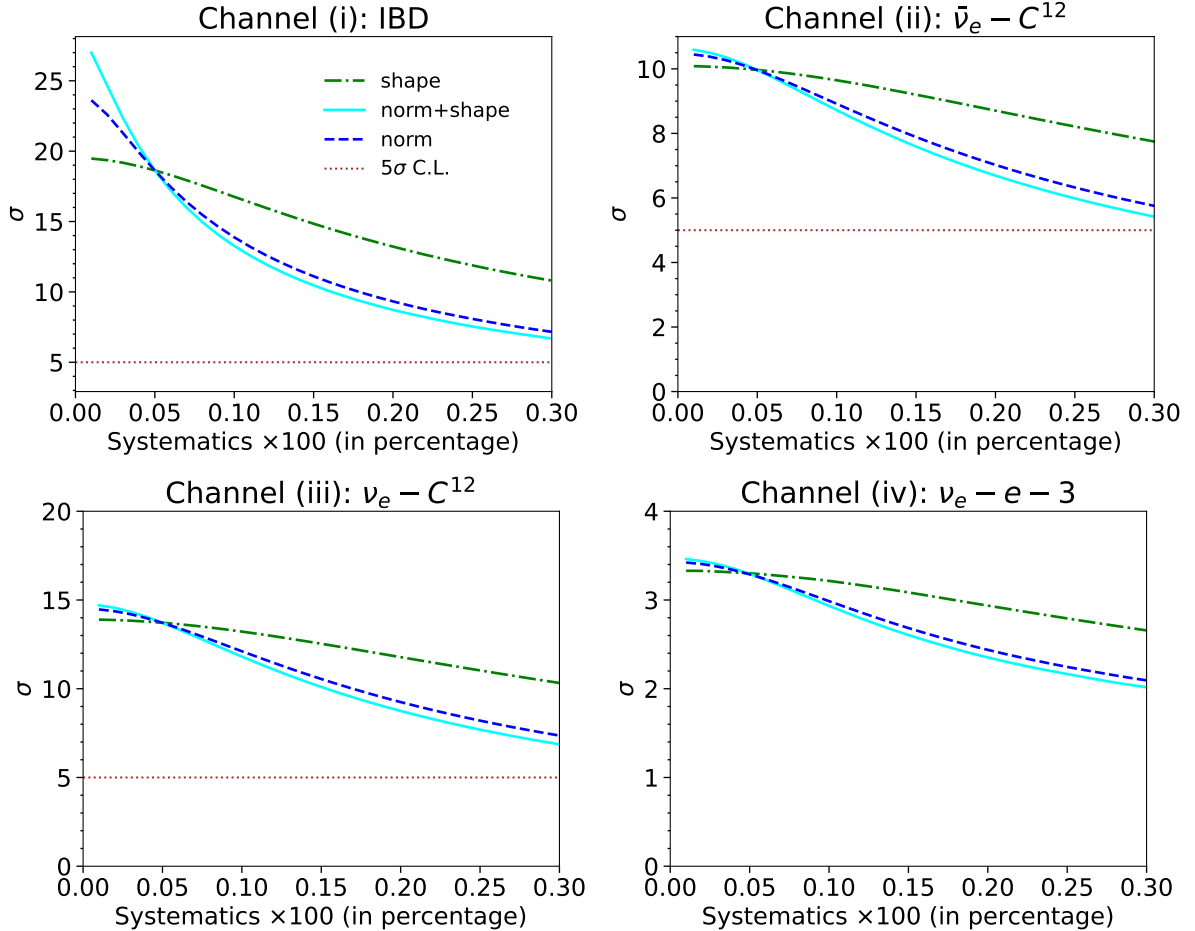


FIG. 7: Mass hierarchy sensitivity as a function of systematic uncertainty (in percentage) at supernova distance of 1 kpc for different conditions. This figure is for active-active framework. However, similar nature is for active-sterile scenario. Color codes are in the legend.

χ^2 calculation. The figure illustrates that when both uncertainties are considered, the mass hierarchy sensitivity is lower compared to cases where only one uncertainty is present. The blue dashed curve, representing the scenario with no systematic errors, exhibits the highest sensitivity.

Interestingly, normalization errors have a more pronounced impact on hierarchy sensitivity compared to energy calibration errors, as the deterioration in sensitivity is greater when only normalization errors are included. This trend is consistent across all channels and for both active-active and active-sterile frameworks.

To provide a clearer understanding of how systematic errors influence hierarchy sensitivity, we present Fig. 7. In each panel of this figure, the green dot-dashed curve corresponds to scenarios with only energy calibration errors, while the blue dashed curve includes only normalization errors. The cyan solid curve accounts for both errors simultaneously. The

figure depicts mass hierarchy sensitivity as a function of systematic uncertainty, which is varied from 0% to 30%, for a supernova distance of 1 kpc.

As systematic uncertainty increases from 0% to 30%, the sensitivity decreases from 25σ to 12σ for the primary IBD channel. Notably, all error types intersect at a systematic uncertainty of 5%. For the NC channel, however, hierarchy sensitivity remains unaffected by changes in systematic error. This is because the mass hierarchy sensitivity for the active-sterile framework in the NC channel is inherently very small, making it insensitive to the type or magnitude of the systematic error. Thus we do not show that in our result panel. In conclusion, we can say that, systematic uncertainty has a significant impact on the mass hierarchy sensitivity in every channel.

C. Effect of smearing

In any long-baseline neutrino experiment, the energy of the neutrino is determined by measuring the energy of the outgoing leptons. This process inherently leads to a loss of information from the incoming neutrino, a phenomenon referred to as “energy smearing.” The inclusion of energy resolution in the analysis results in a further loss of information in the detector, thereby reducing the sensitivity to the neutrino mass hierarchy.

In this subsection, we investigate the impact of energy smearing on mass hierarchy sensitivity for supernova neutrinos in both active-active and active-sterile frameworks. Fig. 8 illustrates how energy smearing affects the event rate spectrum, comparing the cases with and without smearing. This figure represents the event rate spectra for the active-active framework. Similar effect can also be seen for active-sterile scenario as well. In each panel, the red (purple) and green (blue) curves correspond to the event rates for NH (IH) conditions with the presence (absence) of smearing.

The discussion highlights that for channels (i), (ii), and (iii), the event rate spectra remain similar in shape but shift leftward due to energy smearing, as the smearing reduces the reconstructed energy of events. In contrast, for channel (iv), energy smearing modifies the shape of the event rate spectrum. Similarly, for the NC channel, the spectrum becomes more compact with energy smearing, whereas, without smearing, the spectrum is more widely spread.

Next, Figure 9 illustrates the impact of smearing on mass hierarchy sensitivity as a function of supernova distance. The results show that energy smearing reduces the sensitivity across all the channels. Improved energy resolution enhances sensitivity to the mass hierarchy.

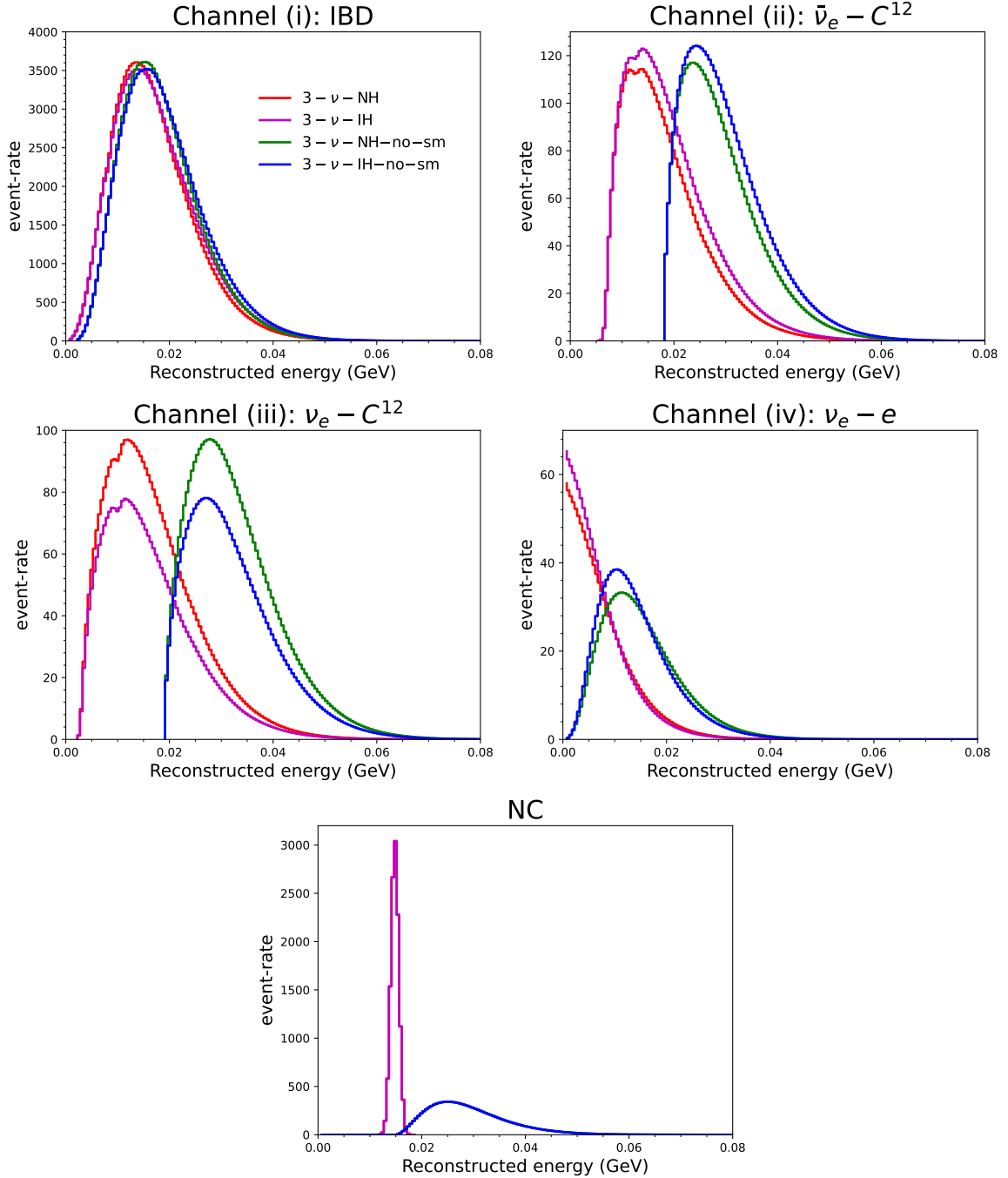


FIG. 8: Event rate for active-active framework as a function of neutrino energy (GeV) for all the main channels and NC. Similar nature has been shown for active-sterile scenario also. Here sm [no-sm] refers to the terms with [without] smearing matrix. Color codes are given in the legend of each panel.

VII. CONCLUDING REMARKS

This work presents a detailed analysis of mass hierarchy sensitivity using supernova neutrinos within the active-active and active-sterile frameworks, focusing on the context of the $\text{NO}\nu\text{A}$ experiment. We investigate the prospects of determining the neutrino mass ordering with the $\text{NO}\nu\text{A}$ detector, considering the possibility that a supernova explosion might occur within the next five years. In such an event, $\text{NO}\nu\text{A}$ could provide valuable insights into mass hierarchy sensitivity through supernova neutrino observations.

This study also explores the impact of sterile neutrinos on mass hierarchy sensitivity. Specifically, if sterile neutrinos exist and were not present at the supernova core initially, but some active supernova neutrinos convert into sterile neutrinos before reaching the detector, we investigate how this transformation influences sensitivity. For the first time, the neutral current (NC) channel is used to distinguish between active and sterile neutrinos. Notably,

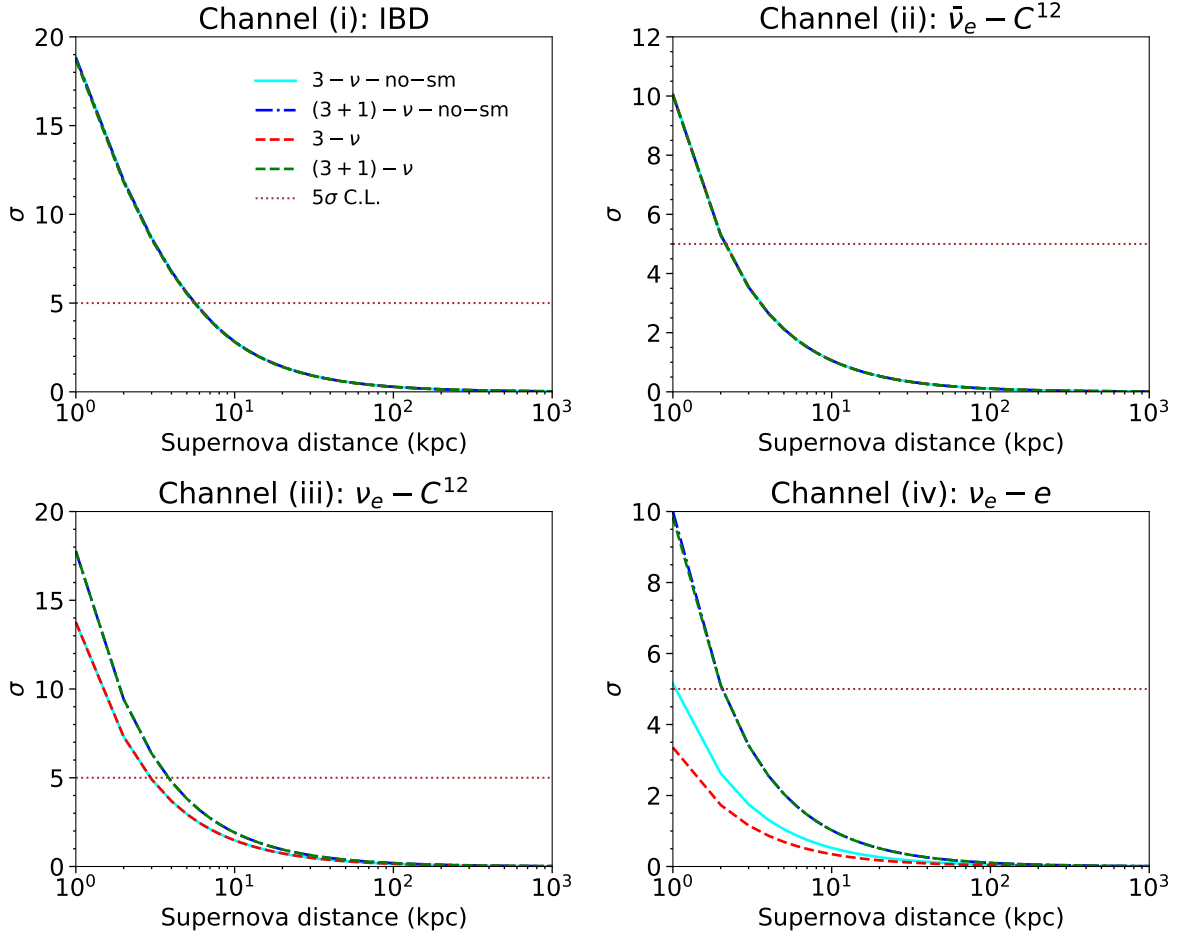


FIG. 9: Mass hierarchy sensitivity as a function of supernova distance (in kpc) with [without] smearing matrix condition for all the channels. Here sm [no-sm] refers to the terms with [without] smearing matrix. Color codes are given in the legend of each panel.

the total NC event rate for the $\bar{\nu}_x - {}^{12}\text{C}$ channel is same in the active-sterile framework as in the active-active scenario. A closer examination reveals that the interplay between the neutrino fluence and the NC cross-section produces this outcome.

The study also compares mass hierarchy sensitivity as a function of supernova distance for both active-active and active-sterile scenarios. The results show that the presence of sterile neutrinos enhances sensitivity for channels (iii) and (iv). Considering NC channel, although active-active scenario is blind on hierarchy conditions, there is a non-zero mass hierarchy sensitivity in active-sterile framework. The mass hierarchy coming from the NC channel is not that significant in the case of $\text{NO}\nu\text{A}$, but the efficient effect can be seen in future experiments with a large detector volume. The effect of systematic errors is also examined, demonstrating that the “no-sys” condition yields the highest sensitivity values, while the inclusion of any systematic errors reduces sensitivity across all channels. Finally, the impact of energy smearing on sensitivity is explored. The results consistently show that non-zero energy resolution decreases sensitivity.

VIII. ACKNOWLEDGMENTS

PP wants to acknowledge Prime Minister’s Research Fellows (PMRF) scheme for financial support. RM would like to acknowledge University of Hyderabad IoE project grant no: RC1-20-012. We gratefully acknowledge the use of CMSD HPC facility of University of Hyderabad to carry out the computational works. We also acknowledge Samiran Roy for useful discussions.

-
- [1] A. A. Aguilar-Arevalo *et al.* (MiniBooNE), *Phys. Rev. Lett.* **121**, 221801 (2018), arXiv:1805.12028 [hep-ex].
 - [2] M. Dentler, A. Hernández-Cabezudo, J. Kopp, P. A. N. Machado, M. Maltoni, I. Martínez-Soler, and T. Schwetz, *JHEP* **08**, 010 (2018), arXiv:1803.10661 [hep-ph].
 - [3] M. M. Saez, M. E. Mosquera, and O. Civitarese, *Int. J. Mod. Phys. E* **31**, 2250023 (2022), arXiv:2109.06244 [hep-ph].
 - [4] A. Esmaili, O. L. G. Peres, and P. D. Serpico, *Phys. Rev. D* **90**, 033013 (2014), arXiv:1402.1453 [hep-ph].
 - [5] A. Boyarsky, O. Ruchayskiy, and M. Shaposhnikov, *Ann. Rev. Nucl. Part. Sci.* **59**, 191 (2009), arXiv:0901.0011 [hep-ph].
 - [6] I. Tamborra, G. G. Raffelt, L. Hudepohl, and H.-T. Janka, *JCAP* **01**, 013 (2012), arXiv:1110.2104 [astro-ph.SR].
 - [7] M.-R. Wu, T. Fischer, L. Huther, G. Martínez-Pinedo, and Y.-Z. Qian, *Phys. Rev. D* **89**, 061303 (2014), arXiv:1305.2382 [astro-ph.HE].

- [8] M. L. Warren, M. Meixner, G. Mathews, J. Hidaka, and T. Kajino, *Phys. Rev. D* **90**, 103007 (2014), arXiv:1405.6101 [astro-ph.HE].
- [9] G. H. Collin, C. A. Argüelles, J. M. Conrad, and M. H. Shaevitz, *Phys. Rev. Lett.* **117**, 221801 (2016), arXiv:1607.00011 [hep-ph].
- [10] A. V. Yudin, D. K. Nadyozhin, V. V. Khruschov, and S. V. Fomichev, *Astron. Lett.* **42**, 800 (2016), arXiv:1701.04713 [astro-ph.HE].
- [11] T. Franarin, J. H. Davis, and M. Fairbairn, *JCAP* **09**, 002 (2018), arXiv:1712.03836 [astro-ph.HE].
- [12] Y. Qian, *Sci. China Phys. Mech. Astron.* **61**, 049501 (2018), arXiv:1801.09554 [astro-ph.HE].
- [13] M. M. Saez, O. Civitarese, and M. E. Mosquera, *Int. J. Mod. Phys. D* **27**, 1850116 (2018), arXiv:1808.03249 [hep-ph].
- [14] J. Tang, T. Wang, and M.-R. Wu, *JCAP* **10**, 038 (2020), arXiv:2005.09168 [hep-ph].
- [15] M. M. Saez, K. J. Fushimi, M. E. Mosquera, and O. Civitarese, *Int. J. Mod. Phys. E* **30**, 2150028 (2021), arXiv:2105.03202 [nucl-th].
- [16] K. J. Fushimi, M. M. Saez, M. E. Mosquera, and O. Civitarese, *Int. J. Mod. Phys. E* **30**, 2150107 (2021), arXiv:2202.03887 [hep-ph].
- [17] G. Chauhan, S. Horiuchi, P. Huber, and I. M. Shoemaker, (2023), arXiv:2309.05860 [hep-ph].
- [18] A. B. Balantekin, G. M. Fuller, A. Ray, and A. M. Suliga, *Phys. Rev. D* **108**, 123011 (2023), arXiv:2310.07145 [hep-ph].
- [19] J. Fetter, G. C. McLaughlin, A. B. Balantekin, and G. M. Fuller, *Astropart. Phys.* **18**, 433 (2003), arXiv:hep-ph/0205029.
- [20] I. Tamborra, *J. Phys. Conf. Ser.* **375**, 042038 (2012).
- [21] M. A. Acero *et al.* (NOvA), *JCAP* **10**, 014 (2020), arXiv:2005.07155 [physics.ins-det].
- [22] J. A. Vasel, *NOvA as a Supernova Observatory*, Ph.D. thesis, Indiana U. (2021).
- [23] X.-R. Huang, C.-L. Sun, L.-W. Chen, and J. Gao, *JCAP* **09**, 040 (2023), arXiv:2305.00392 [hep-ph].
- [24] A. L. De Santis, *Nuovo Cim. C* **47**, 303 (2024).
- [25] L. Pattavina *et al.* (RES-NOVA), *JCAP* **10**, 064 (2021), arXiv:2103.08672 [astro-ph.IM].
- [26] M. A. Acero *et al.* (NOvA), *Phys. Rev. D* **104**, 063024 (2021), arXiv:2106.06035 [hep-ex].
- [27] P. Panda, M. Ghosh, and R. Mohanta, *JCAP* **10**, 033 (2023), arXiv:2304.13303 [hep-ph].
- [28] R. Gaba, M. Mukherjee, and V. Bhatnagar, (2024), arXiv:2411.07716 [hep-ph].
- [29] A. Mirizzi, I. Tamborra, H.-T. Janka, N. Saviano, K. Scholberg, R. Bollig, L. Hudepohl, and S. Chakraborty, *Riv. Nuovo Cim.* **39**, 1 (2016), arXiv:1508.00785 [astro-ph.HE].
- [30] A. S. Dighe and A. Y. Smirnov, *Phys. Rev. D* **62**, 033007 (2000), arXiv:hep-ph/9907423.
- [31] L. Wolfenstein, *Phys. Rev. D* **17**, 2369 (1978).
- [32] S. P. Mikheev and A. Y. Smirnov, *Sov. Phys. Usp.* **30**, 759 (1987).
- [33] L. Hudepohl, B. Muller, H. T. Janka, A. Marek, and G. G. Raffelt, *Phys. Rev. Lett.* **104**, 251101 (2010), [Erratum: *Phys.Rev.Lett.* 105, 249901 (2010)], arXiv:0912.0260 [astro-ph.SR].

- [34] S. Chakraborty, R. Hansen, I. Izaguirre, and G. Raffelt, Nucl. Phys. B **908**, 366 (2016), arXiv:1602.02766 [hep-ph].
- [35] S. Horiuchi and J. P. Kneller, J. Phys. G **45**, 043002 (2018), arXiv:1709.01515 [astro-ph.HE].
- [36] I. Tamborra and S. Shalgar, Ann. Rev. Nucl. Part. Sci. **71**, 165 (2021), arXiv:2011.01948 [astro-ph.HE].
- [37] D. S. Ayres *et al.* (NOvA), (2007), 10.2172/935497.
- [38] P. Adamson *et al.* (NOvA), Phys. Rev. D **93**, 051104 (2016), arXiv:1601.05037 [hep-ex].
- [39] P. Adamson *et al.* (NOvA), Phys. Rev. Lett. **118**, 151802 (2017), arXiv:1701.05891 [hep-ex].
- [40] P. Adamson *et al.* (NOvA), Phys. Rev. Lett. **118**, 231801 (2017), arXiv:1703.03328 [hep-ex].
- [41] M. A. Acero *et al.* (NOvA), Phys. Rev. D **98**, 032012 (2018), arXiv:1806.00096 [hep-ex].
- [42] M. A. Acero *et al.* (NOvA), Phys. Rev. Lett. **123**, 151803 (2019), arXiv:1906.04907 [hep-ex].
- [43] S. Mufson *et al.*, Nucl. Instrum. Meth. A **799**, 1 (2015), arXiv:1504.04035 [physics.ins-det].
- [44] I. Esteban, M. C. Gonzalez-Garcia, M. Maltoni, T. Schwetz, and A. Zhou, JHEP **09**, 178 (2020), arXiv:2007.14792 [hep-ph].
- [45] <http://www.phy.duke.edu/schol/snowglobes>, “Github,” (2021).
- [46] P. Huber, M. Lindner, and W. Winter, Comput. Phys. Commun. **167**, 195 (2005), arXiv:hep-ph/0407333.
- [47] P. Huber, J. Kopp, M. Lindner, M. Rolinec, and W. Winter, Comput. Phys. Commun. **177**, 432 (2007), arXiv:hep-ph/0701187.
- [48] M. C. Gonzalez-Garcia and M. Maltoni, Phys. Rev. D **70**, 033010 (2004), arXiv:hep-ph/0404085.